Structure and properties of P^+-ion-implanted polycrystalline iron films

1989 J. Phys.: Condens. Matter 1 6787

(http://iopscience.iop.org/0953-8984/1/38/003)

J. Phys.: Condens. Matter 1 (1989) 6787–6792. Printed in the UK

Structure and properties of P^+-ion-implanted polycrystalline iron films

Liang-Mo Mei, Xiao-Gin Guo and Yue-Lu Zhang
Department of Physics, Shandong University, Jinan, Shandong, People's Republic of China

Received 10 January 1989, in final form 30 March 1989

Abstract. The structures and properties of polycrystalline iron films implanted with P^+ ions have been studied. The electrical resistance, the magnetic coercive force and the permeability of the film, as functions of the P^+ ion dose, have been measured and their variations with the dose seem to be universal for the stress release–defect accumulation–lattice collapse process. The results can be described by the critical-defect-density model of amorphisation.

1. Introduction

The amorphous materials developed recently (in particular, amorphous alloys which constitute a major class) have been one of the subjects studied extensively in solid state physics. However, the formation process of amorphous materials remains ambiguous so far because it was very difficult to study it in the earliest melt-quenching method. The preparation technique for amorphous materials by implanting high-dose ions into transition metals can offer us a series of intermediate stable or metastable states from crystalline to amorphous which give a new insight into the amorphisation mechanism and the microscopic structure of amorphous alloys.

A number of papers on the formation of amorphous alloys by ion implantation have been published [1–8]; most of them have dealt with the amorphisation conditions and the observation of structures and only a few have involved the physical properties of ion-implanted layers. Research on the magnetic properties and the relationship between these properties and the structures is basically virginal. So in this paper the measurement of some physical properties and the observation of the structures of P^+-ion-implanted films were carried out at the same time so as to be able to obtain more information about the crystalline-to-amorphous transition and to compare this with our early experimental results on the implantation of B^+ ions [9].

2. Sample preparation

The polycrystalline iron films were prepared by vacuum evaporation deposition on freshly split NaCl single crystal or polished single-crystal silicon wafers; the former were used for transmission electron microscopy (TEM) and x-ray diffraction, and the latter for other measurements. During deposition the substrate was heated to about 200 °C and

0953-8984/89/386787 + 06 $02.50

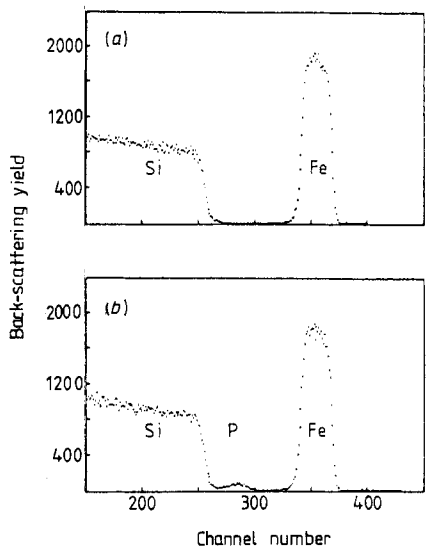

Figure 1. RBS spectra of the iron film (*a*) before and (*b*) after implantation of 100 keV P^+ ions at a dose of 1×10^{17} ions cm^{-2} (film thickness, 1050 Å; analysing particles, 2 MeV $^4He^{2+}$; back-scattering angle, 135°; channel width, 3.58 keV).

the deposition rate was about 1 Å s^{-1}. The film thickness was monitored and measured using a quartz crystal oscillator. For a film of nominal thickness $d = 1050$ Å, a Rutherford back-scattering spectroscopy (RBS) experiment was carried out; the back-scattering energy spectrum of α-particles is shown in figure 1(*a*) from which the film thickness can be derived to be 998 Å, which is in good agreement with the result obtained using the quartz crystal oscillator.

The implanted ion energy was selected so that the mean projected range R_p of the ions was at about the middle of the film, i.e. $d \simeq 2R_p + \Delta R_p$, where ΔR_p is the standard deviation of the projected range. The ion implantation was carried out on a MPB-200 implanter with ions of two energies, 70 keV and 100 keV, at a pressure of 2×10^{-7} Torr in the target chamber. The mean current density and the scanning non-uniformity were 1.5 μA cm^{-2} and 3%, respectively. The temperature of the sample during implantation was kept below 50 °C.

The experiments on RBS and secondary-ion mass spectrometry (SIMS) have shown that the distribution of the ions in the implanted layer was of a Gaussian type up to a dose D of 10×10^{16} ions cm^{-2}. Figure 1(*b*) shows the RBS spectrum of the implanted film. For the film implanted with 100 keV ions, the distribution parameters derived from the experiments, $R_p = 520$ Å and $\Delta R_p = 250$ Å, were basically consistent with those calculated from the LSS theory [10], $R_p = 477$ Å and $\Delta R_p = 232$ Å, indicating that the influences of surface sputtering and radiation-enhanced diffusion during implantation were not serious.

3. Structure observation

The polycrystalline structure of the as-deposited films were demonstrated by the TEM images and selected-area diffraction (SAD) patterns (figure 2(*a*)). After implantation of low-dose P^+ ions ($D = 10^{16}$ ions cm^{-2}), the crystallite boundaries become clearer and some of the crystallites grew larger. At the same time, more diffraction rings with sharper fringes could be seen (figure 2(*b*)), but no new phases appeared. This result can be

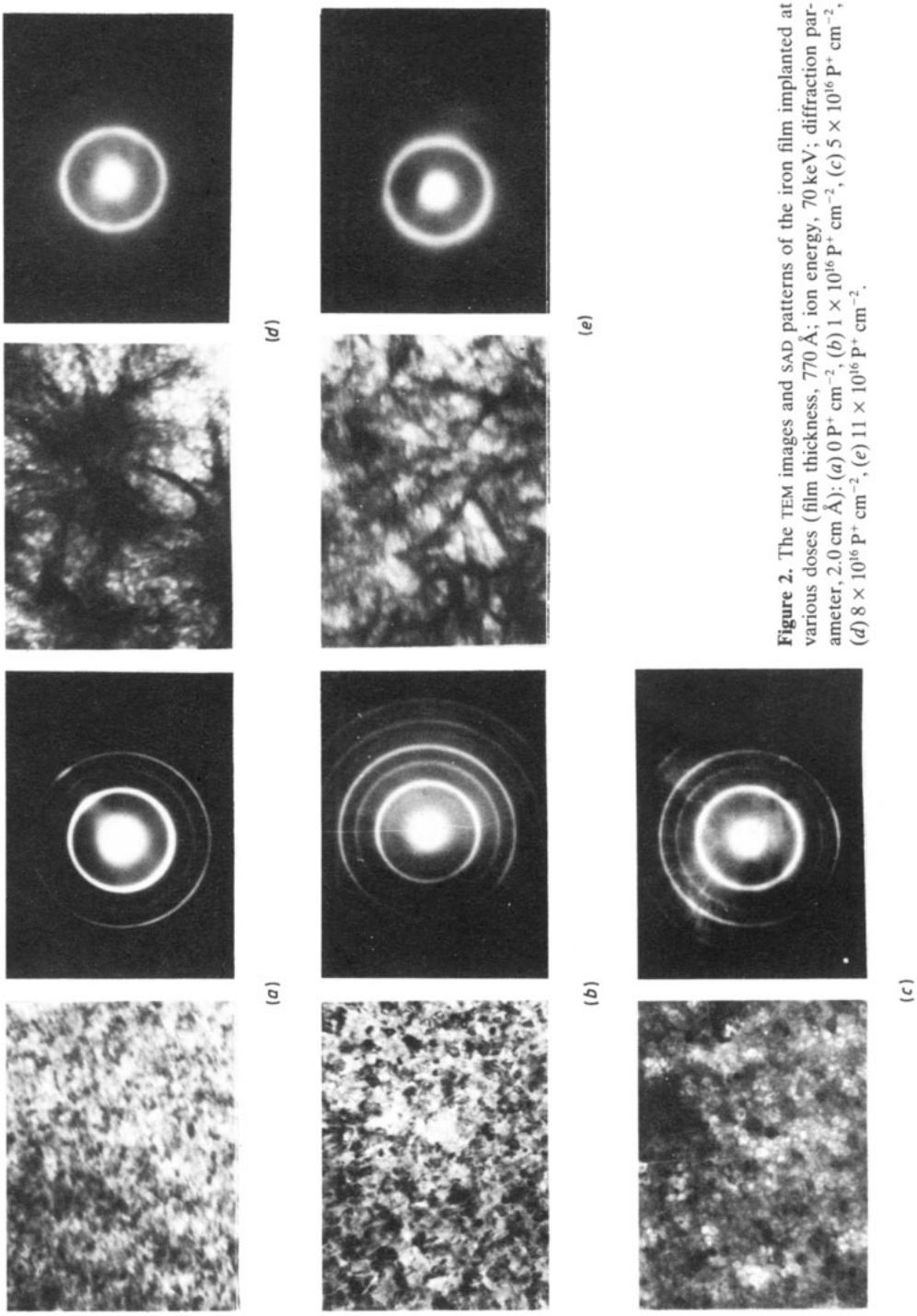

Figure 2. The TEM images and SAD patterns of the iron film implanted at various doses (film thickness, 770 Å; ion energy, 70 keV; diffraction parameter, 2.0 cm Å): (*a*) 0 P^+ cm^{-2}, (*b*) 1×10^{16} P^+ cm^{-2}, (*c*) 5×10^{16} P^+ cm^{-2}, (*d*) 8×10^{16} P^+ cm^{-2}, (*e*) 11×10^{16} P^+ cm^{-2}.

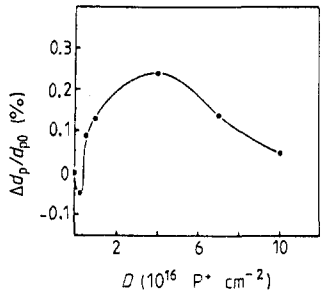

Figure 3. Relative increment in the lattice parameter d_p as a function of the dose D (d = 1050 Å; E = 100 keV; x-ray Fe K; d_{p0} = 2.030 Å (as-deposited film)).

explained in terms of the annealing effect of the ions produced by the intense migration of the atoms under ion bombardment.

In the medium-dose range (D = (2–5) × 10^{16} ions cm^{-2}), the TEM pictures look like tangled hemp (figure 2(d)) and the diffraction rings also become fewer and dimmer (see figure 2(c)), which can be explained in terms of the emergence of a large quantity of primary defects under bombardment of the implanted ions and formation of complex defects which were stabilised by the implanted impurity atoms. As the P^+ ion dose was increased further, the crystalline grains and the corresponding diffraction rings disappeared gradually and one or two diffuse rings appeared (figure 2(d)); this shows that the amorphous state starts to form in some areas. At the highest dose (D = 11 × 10^{16} ions cm^{-2}), only diffuse rings can be seen in the SAD patterns, indicating that the amorphous state has been the main structure of the film.

The above observed results are similar to the B^+-ion-implanted iron case; therefore, it can also be described in terms of the critical defect density model. However, the size and the density of the defects in P^+-ion-implanted iron films are both smaller than in B^+-ion-implanted iron, indicating that P^+ is less effective than B^+ in stabilising defects in the iron metal.

The lattice parameter d_p of the most densely arranged atomic planes, calculated from the positions of the x-ray diffraction lines, as a function of the dose D is shown in figure 3. The variation in d_p with dose can be divided into three stages. When the P^+ ion dose is low, d_p decreases slightly with increasing dose and its minimal value is 2.029 Å which equals that derived from standard density of the iron, indicating that in this stage the ion-annealing effect caused by partly eliminating the stresses or reducing the lattice deformation plays a more important role than does the radiation damage. In the medium-dose range, however, owing to the defect accumulation in the implanted film the crystal lattices were deformed heavily; as a result, d_p increases with increasing P^+ ion dose and reaches its maximum at about D = 5 × 10^{16} ions cm^{-2}. Then d_p decreases again, indicating that the high-density accumulation of the defects has led to lattice collapse and formation of the amorphous state in which the average packing density of atoms is higher than that of the high-defect-density regions. Finally, d_p tends to a constant value, indicating that the film has been amorphised completely. The above experimental results are very similar to those for B^+-ion-implanted niobium in [11].

4. Measurements of physical properties

Some physical properties of the implanted film—the resistance R, the magnetic coercive force H_c and the permeability μ—as functions of the P^+ ion dose are shown in figure 4.

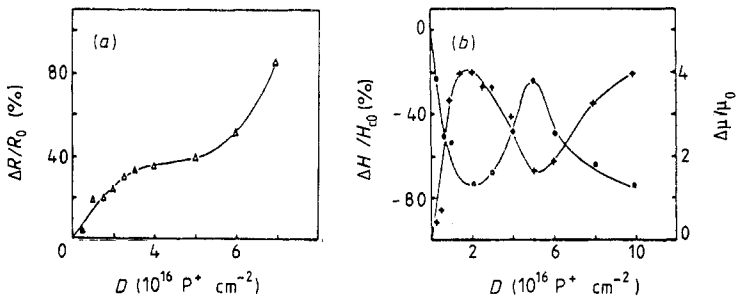

Figure 4. The relative increments in (*a*) R, and (*b*) H_c (●) and μ (+) for the film as functions of the dose D (the film thickness d = 1050 Å; E = 100 keV; as-deposited film parameters R_0 = 30 Ω, H_{c0} = 30 Oe and μ_0 = 150; testing frequency, DC for R, 50 Hz for H_c and 13 MHz for μ).

Similarly, their variations with the P^+ ion dose can be divided into three stages. In the low-dose range, because of the existence of point defects produced by radiation damage, R increases linearly with increasing dose, while H_c decreases and μ increases, indicating that, for some magnetic properties which are sensitive to the structure, the stress release caused by ion annealing is more important than radiation damage. In the medium-dose range, because the complex defects were less effective in scattering electrons than are the point defects, the increasing rate of R with increasing dose is slowed down. The accumulating defects make the film heterogeneous and thus H_c increases and μ decreases whereas, once the defect density reaches a critical value, the crystal lattices start to collapse and form amorphous areas which possess a higher resistance as a result, leading to a very rapid increase in R. However, owing to the absence of grain boundaries and the low anisotropy in amorphous state, H_c decreases and μ increases again.

5. Theoretical considerations

From the analyses of the structure and the physical properties, the critical dose D_c of amorphisation can be determined to be about 5×10^{16} ions cm^{-2}, higher than that for B^+-ion-implanted iron [9]. The P^+ ion distribution profile can be described by a Gaussian curve approximately (LSS theory) [12]:

$$N(x) = [D/\sqrt{(2\pi)\,\Delta R_p}]\exp[-(x - R_p)^2/2\,\Delta R_p^2] \tag{1}$$

which has been proved by the RBS and SIMS experiments. So, when $D = D_c$, the peak value of P^+ concentration in the implanted film is about 10 at.%, corresponding to the lowest phosphorus concentration required to stabilise the amorphous structure in quenched Fe–P ribbon. Therefore, it is reasonable to assume that amorphisation occurs at about the mean projected range of the ions first and then extends to the two sides constantly. Now, according to this model, the effective thickness x_a of the amorphous layer at the highest dose D_{max} can be derived; this is

$$x_a = 2\,\Delta R_p\sqrt{2\ln(-D_{max}/D_c)}. \tag{2}$$

For E = 100 keV and $D_{max} = 10^{17}$ P^+ cm^{-2}, ΔR_p = 250 Å and $D_c = 5 \times 10^{16}$ P^+ cm^{-2}, so that x_a = 640 Å. When we take into account that the iron film was thinned about 80 Å by the sputtering effect of the ions, the amorphous fraction in the implanted film is about

65%; this is in agreement with the x-ray diffraction data which show that the diffraction peak intensity of the remaining crystalline iron is equal to 40% of that before implantation.

6. Conclusions

(i) The variations in the microscopic structure observed by TEM and x-ray diffraction can be explained in terms of ion annealing, radiation damage and crystal lattice collapse. Thus the amorphisation mechanism can be described by the critical defect density model.

(ii) Some physical properties are governed by stress release, defect accumulation and amorphous state formation produced in the ion implantation process.

(iii) It seems that the above experimental results are common to the implantation of metalloid ions into as-deposited ferromagnetic transition metal films.

References

[1] Ali A,Grant W A and Grundy P J 1978 *Phil. Mag.* B **37** 353
[2] Traverse A and Ruault M O 1982 *Metastable Materials Formation By Ion Implantation* ed. S T Picraux and W J Choyke (Amsterdam: Elsevier) p 217
[3] Mendoza-Zelis L, Thome L, Brossard L, Chaumont J, Krolas K and Bernas H 1982 *Phys. Rev.* B **26** 1306
[4] Rauschenbach B and Hohmuth K 1982 *Phys. Status Solidi* a **72** 667 (in German)
[5] Tsukahara S and Kanayama T 1983 *J. Magn. Magn. Mater.* **31–4** 927
[6] Kolitsch A, Rauschenbach B and Richter E 1983 *Radiat. Eff. Lett.* **76** 193
[7] Al-Tamimi Z Y, Grant W A and Grundy P J 1984 *Vacuum* **34** 861
[8] Cohen C, Benyagoub A, Bernas H, Chaumont J, Thome L, Berti M and Drigo A V 1985 *Phys. Rev.* B **31** 5
[9] Mei L M, Zhang Y L, Kuo Y C and Guo X G 1986 *J. Magn. Magn. Mater.* **59** 346
[10] Chu W K, Mayer J W and Nicolet M A 1978 *Backscattering Spectrometry* (New York: Academic) p 63
[11] Linker G 1985 *Mater. Sci. Eng.* **69** 105
[12] Rauschenbach B, Blasek G and Dietsch R 1984 *Phys. Status Solidi* a **85** 473